Compact QEPAS sensor for trace methane and ammonia detection in impure hydrogen

Lei Dong[1], Jonathan Wright[2], Brent Peters[2], Blythe Ferguson[2], Frank K. Tittel[1], Scott McWhorter[2]

[(1)]Rice University, Department of Electrical and Computer Engineering, 6100 Main Street, Houston TX 77005, USA

[(2)] Hydrogen Technology Research Laboratory, Savannah River National Laboratory, Aiken, SC 29808, USA

Abstract. A compact two-gas sensor based on quartz enhanced photoacoustic spectroscopy (QEPAS) was developed for trace methane and ammonia quantification in impure hydrogen. The sensor is equipped with a micro-resonator to confine the sound wave and enhance QEPAS signal. The normalized noise-equivalent absorption coefficients (1σ) of 2.45×10^{-8} $cm^{-1}W/\sqrt{Hz}$ and 9.1×10^{-9} $cm^{-1}W/\sqrt{Hz}$ for CH_4 detection at 200 Torr and NH_3 detection at 50 Torr were demonstrated with the QEPAS sensor configuration, respectively. The influence of water vapor on the CH_4 channel was also investigated.

PACS 42.55.Px; 82.80.Kq; 42.62.Fi;

1. Introduction

The development of robust and compact optical sensors for muti-gas detection is of considerable interest in diverse applications, such as gas purity measurements, industrial processing control, environmental monitoring and medical diagnostics. Quartz enhanced photoacoustic spectroscopy (QEPAS) is a rapidly developing, sensitive, selective spectroscopic technique for laser based trace gas detection with a fast response time [1, 2]. QEPAS combines the main characteristics of photoacoustic spectroscopy (PAS) with the benefits of using a quartz tuning fork (QTF), thus providing an ultra-compact, cost-effective, robust acoustic detection module (ADM). Moreover, QEPAS can achieve sensitivities comparable to conventional PAS, but with reduced ambient acoustic noise due to the acoustic quadrupole nature of the QTF [3].

The micro-resonator (mR) plays a crucial role in QEPAS sensors and acts similarly to the acoustic resonator in conventional PAS [4]. In the QEPAS sensor architecture, the mR consists of two rigid hypodermic tubes that surround the QTF. The energy of the acoustic wave induced by radiation excitation is accumulated in the mR by means of the resonant effect and subsequently transferred to the QTF as the result of coupling between the mR and QTF. Recent studies reported that the optimum length of each mR tube is between $\lambda_s/4$ and $\lambda_s/2$ where λ_s is the

wavelength of sound [3, 5]. The results reported in Ref 3 showed that an optimized mR configuration can further improve the QEPAS signal-to-noise ratio (SNR) by up to 30 times, as compared to using a bare QTF.

To date, the QEPAS sensor technique has been employed to detect, monitor and quantify several molecules with well resolved rotational-vibrational lines in the near-infrared spectral range (e.g., NH_3, CO_2, CO, HCN, HCl, H_2O, H_2S, CH_4, C_2H_2, C_2H_4) [6-10] as well as in the mid-infrared spectral region (e.g., NO, N_2O, CO, NH_3, C_2H_6, and CH_2O) [11-16]. QEPAS has also been demonstrated with larger molecules with broad, unresolved absorption spectra, such as ethanol, acetone and freon [17]. However, QEPAS based sensors reported above were primarily developed for monitoring target gas concentrations while using N_2 or air as the carrier gas. Carrier gas choice is critical; the QEPAS sensor detection sensitivity can be affected by the conversion efficiency of the absorbed optical radiation power into the sound energy, which is determined by the vibrational-to-translational (V-T) energy transfer rate of the target gas. This rate usually changes with different carrier gases and also in the presence of H_2O vapor, which is an efficient catalyst for the vibrational energy transfer reactions in the gas phase.

Detection and quantitative measurement of trace impurities including CH_4 and NH_3 in hydrogen gas process streams is of critical importance to refinement and purification of hydrogen isotopologues at the Savannah River National Laboratory (SRNL), Aiken, SC. The QEPAS technique presents a unique, new methodology for impurity analysis within impure hydrogen gas streams. Because the parameters and the performance of mR are strongly dependent on the properties of the carrier gas, in particular the gas density, speed of sound, and relative humidity within the gas, the mR parameters must be reconsidered in order to meet application needs of specific gas environments such as H_2. The reported speed of sound in hydrogen is 1330 m/s at room temperature [18] which is ~4 time faster than in air, since the density of H_2 is only 1/14 of the density of air. Thus, the mR used in N_2 or air is no longer optimized when H_2 is the carrier gas. The mR parameters must be reoptimized in order to meet the requirement of the H_2 carrier gas environment. In this work, we report the design, development and optimization of a compact two-gas QEPAS-based sensor for detection and monitoring of trace methane (CH_4) and ammonia (NH_3) concentration in impure hydrogen. We also performed a side-by-side inter-comparison between the new QEPAS sensor and the previously reported QEPAS sensor designed for detecting trace CH_4 and NH_3 in H_2 and in N_2 carriers, respectively.

2. Sensor design

The diode laser based QEPAS sensors employ commercially available QTFs that are designed for use as the frequency reference at a resonant frequency of ~32.8 kHz. The speed of sound at room temperature was in air is ~340 m/s [18]. Based on Ref. [3, 19], the empirically determined optimum mR tube length was 4.4 mm in N_2, which is between $\lambda_s/4$ and $\lambda_s/2$, as mentioned above. The optimum mR tube inner diameter was ~0.5 mm. However, with hydrogen as the carrier gas, the estimated optimum mR tube length was ~20 mm due to the faster speed of sound in H_2. Thus, the total length of the two mR tubes employed in one ADM for the sensor platforms increased to ~40 mm. This increased mR length represents a challenge to focus the excitation diode laser beam passing through the 40 mm-long mR and the 300 μm gap between the prongs of the QTF without optical contact. In fact, any optical contact between the diode laser excitation radiation and the mR or QTF results in an undesirable, non-zero background. This additional background is several factors larger than the thermal noise level of QEPAS. As a result, the ~20mm optimized mR tube length (which must be matched to the acoustic wavelength so that the acoustic energy can be efficiently accumulated in the mR tube) is no longer suitable for QEPAS-based trace gas detection in H_2

In previous QEPAS based sensor studies, it was observed that a non-matched length short mR can still increase the QEPAS sensitivity by a factor of 10 times or more [2, 16]. In this case, the mR tubes act to confine the sound wave, but do not exhibit a well defined resonant behavior. Therefore we adopted a non-matched mR configuration for the QEPAS based sensor used to detect trace gases in a H_2 carrier gas. Two 5 mm-long mR tubes, whose length is 4 times smaller than the evaluated 20 mm optimum length, were employed. The mR tubes featured an inner tube diameter of 0.58 mm and outer tube diameter of 0.9 mm

A typical acoustic detection module (ADM) for a QEPAS-based sensor incorporates a QTF, mR tubes and an enclosure that allows operation at a reduced pressure determined for the targeted trace gas mixture. A fiber-coupled ADM was used in the sensor, depicted in Fig.1. This ADM was assembled in a telecom-style butterfly package by Achray Photonics, Inc. The near infrared radiation was delivered to the ADM via a single mode optical fiber and then focused by a GRAIN lens. Active optical alignment was used to ensure free propagation of the radiation through the mR tubes. Epoxy was used to attach both the QTF and the mR tubes to the metallic mount.

The QEPAS sensor system shown in Fig.2 consists of three parts: a control electronics unit (CEU) [1], an ADM, and a switching module. The diode laser for NH_3 detection (JDS Uniphase, CQF 935.908-19570) and two reference cells (Wavelength References, Inc) for CH_4 and NH_3 monitoring were mounted inside the CEU. An electronic switchboard to select the appropriate signal from one of the two reference cells was also incorporated into the CEU. The CEU was

responsible for measuring the basic QTF parameters (the resonant frequency f_0, quality factor Q and resistance R of the QTF), modulating the two diode lasers at half the resonant frequency of the QTF frequency for optimum detection sensitivity, and locking of the laser wavelength to a selected absorption line of the target analyte. To determine the QTF parameters, a sine wave excitation voltage was applied to the QTF electrodes, and the excitation frequency was scanned to determine the QTF resonant frequency by measuring the QTF current. The Q factor was derived from the QTF ring-down time following a rapid interruption of the excitation voltage. The diode laser for CH_4 detection (NEL, NLK1U5FAAA) and a 4×4 MEMs optical switch were mounted in the switching module. The 4×4 MEMS switch was realized by combining two 1×4 switches (LightBand Mini 1×4, Agiltron Inc.). The MEMs switch was controlled to direct either of the two diode lasers to the ADM via a parallel 4-bit binary code provided by the CEU. The QEPAS based sensor head consisted of the ADM and a compact enclosure in which ultra small temperature, pressure and humidity sensors were mounted. Finally, a notebook PC computer communicated with the CEU via a RS232 serial port for collection of 2f harmonic data and gas temperature, humidity, pressure parameters.

3. Signal amplitude and noise sources of QEPAS

The QEPAS signal S_{QEPAS} can be expressed as [19]

$$S_{\mathrm{QEPAS}} = C_{\mathrm{ADM}} P_0 C Q(p) \alpha(p) \varepsilon(p), \tag{1}$$

where C_{ADM} is the ADM constant, P_0 is the incident optical power, C is the detected gas concentration, Q is the quality factor of the QTF, α is the peak intensity of the 2f absorption spectrum, and ε is the conversion efficiency of the absorbed optical radiation power into acoustic energy. Q, α, and ε are pressure dependent. In addition, the peak intensity α, depends on the laser wavelength modulation (WM) depth. When the modulation width is close to the absorption linewidth, the maximum 2f signal is achieved. Therefore in order to optimize the sensor performance, both the gas pressure and the WM depth must be appropriately selected.

Assuming only collision de-excitation between molecules is taken into account, it is known that the conversion efficiency is related to the relaxation time τ of a target gas as follows [20, 21]

$$\varepsilon(p) = \frac{1}{\sqrt{1+\tan^2\theta}}, \tag{2}$$

$$\tan\theta = 2\pi f \tau(p), \tag{3}$$

$$\tau(p) = \frac{P_0 \tau_0}{p}, \tag{4}$$

where θ is the QEPAS signal phase, f is the modulation frequency of the optical excitation, and $P_0\tau_0$ is the relaxation time constant. These equations imply that increasing pressure leads to a corresponding increased rate of molecular collisions and produces a faster V-T relaxation of the target analyte.

A background noise analysis of a QEPAS equivalent circuit shows that two primary noise sources are the thermal noise associated with mechanical dissipation in the QTF, as represented by the R in the series RLC equivalent circuit [1]:

$$\sqrt{< V_{N-R}^2 >} = R_g \sqrt{\frac{4k_B T}{R}} \sqrt{\Delta f}, \tag{5}$$

$$R = \frac{1}{Q}\sqrt{\frac{L}{C}}, \tag{6}$$

and the thermal noise of the feedback resistor:

$$\sqrt{< V_{N-Rg}^2 >} = \sqrt{4k_B T R_g} \sqrt{\Delta f}, \tag{7}$$

where the R_g=10 MΩ is the feedback resistor of transi-mpedance preamplifier, k_B is the Boltzmann constant, T is QTF temperature, and Δf is the detection bandwidth. As the noise caused by feedback resistor R_g is $(R_g/R)^{1/2}$ times lower than the QTF noise, R_g is usually neglected over typical values of R (10 to 200 kΩ). Additionally, it has been verified in previous QEPAS performance tests that the observed QEPAS noise is equal to the theoretical noise of the QTF [4, 11, 19].

4. Optimization and sensitivity of the CH_4 detection channel

The R(4) manifold of the CH_4 $2\nu_3$ band near 6057.1 cm^{-1} was employed as the selected CH_4 detection line. The R(4) manifold consists of four discrete absorption lines. An example of the QEPAS spectra acquired for using 100 ppm CH_4 at 200 Torr H_2 mixture is shown in Fig.3. The four discrete absorption lines are closely spaced so that only one merged line was observed resulting in slight asymmetry at 200 Torr. Due to the absence of the CH_4 broadening coefficient in H_2, it is difficult to obtain the optimum laser WM amplitude for different pressures by numerically simulating the $2f$ line shapes based on the approach described in Ref [19]. Optimization of the gas pressure and the WM depth was carried out experimentally with a 100 ppm (by volume) CH_4 in H_2 mixture. The flow rate was set to 150 sccm.

The CH_4 QEPAS $2f$ signal corresponding to the peak absorption was plotted as a function of gas pressure and laser current modulation depth as shown in Fig. 4 (a). Maximum signal was observed at 200 Torr. The measured Q factors and the R values of the QTF are shown in Fig. 5

(solid lines). The Q factor of a QTF is dependent on the QTF temperature, the surrounding gas pressure. and the property of the major chemical composition of the target analyte. Due to the smaller vibrational damping in H_2 (as compared to N_2), the QTF has a high Q factor (>30,000). The high QTF Q enhances the QEPAS signal amplitude since the QEPAS signal is proportional to the Q factor (Eq. (1)). However, based on Eq. (6), the product of Q and R of the QTF is a constant because the equivalent QTF L and C parameters are constant. As a result, the higher Q factor decreases R, resulting in higher noise contribution. For comparison, at 200 Torr, the noise level (1σ) is 4.8 μV in hydrogen, while it is only 2.7 μV in nitrogen. So in order to appropriately optimize and assess the CH_4 channel performance, both signal and noise should be considered. In Fig. 6(a), the normalized maximum signal amplitude and signal-to-noise ratio (SNR) are plotted as a function of pressure, based on the data in Fig. 4(a) and Eq. (5). The optimum detection pressure for both the CH_4 QEPAS signal amplitude and the SNR occur at ~200 Torr. Unlike CH_4 trace detection in nitrogen [19], the pressure shift for the two optimum detection pressures is not observed. This pressure behavior is due to insensitivity of R to pressure changes in hydrogen. Between 100 to 760 Torr, the R values range from 100 to 230 kΩ in nitrogen, while the R values range from 53 to 86 kΩ in hydrogen. Using Eq. (5), smaller values of R result in a smaller variation of noise level in hydrogen than in N_2. Consequently, the signal amplitude as a function of pressure has the same shape and position as the SNR curve.

Measurements of the CH_4 channel response to different CH_4 concentrations at the optimum pressure of 200 Torr verified the CH_4 channel linearity. The laser wavelength was locked to the center of the 6057.1 cm^{-1} absorption line. Four gas cylinders containing different calibrated CH_4 concentration levels were used to supply the sample gas. The results of measurements performed every 1 s are shown in Fig. 7. These measurements were made for a dynamic range of only 100 because of the limited availability of calibrated gas samples. Previous CO_2 and NO experiments indicated that the linear dynamic range of a QEPAS-based sensor can cover at least 4 orders of magnitude [11] as the QTF is known to be a linear response transducer with a dynamic range of $>10^7$. The absolute detection sensitivity of the QEPAS sensor to CH_4 in dry H_2 was also evaluated. The scatter of consecutive measurements at a certain concentration level did not depend on the concentration. The noise level based on scatter data was 4.6 μV with Δf=0.785 Hz. The calculated noise level was 4.8 μV based on Eq. (5) (R=56.4 kΩ). This agreement confirms that no excess noise is introduced. This noise level results in a noise-equivalent (1σ) concentration of 3.2 ppm with a 1-s averaging time (0.785 Hz). Normalized to 15.8 mW optical power and a 0.785 Hz detection bandwidth, the noise equivalent absorption coefficient is

2.45×10^{-8} $cm^{-1}W/\sqrt{Hz}$. This coefficient is slightly lower when compared with the CH_4 detection sensitivity in dry N_2 (2.9×10^{-8} $cm^{-1}W/\sqrt{Hz}$).

5. CH_4 conversion efficiency in the presence of H_2O vapor

For trace methane in a nitrogen mixture, the observed QEPAS signal generated at a certain CH_4 concentration is much stronger in the presence of H_2O vapor as the water is an efficient catalyst for the vibrational energy transfer reactions in the gas phase. Hence, the influence of H_2O on overall QEPAS signal when using hydrogen as the carrier gas was investigated. First, 2.29% H_2O vapor was added to the 100 ppm dry CH_4 by means of a Nafion tube. The 2*f* peak values were recorded at different pressures and are shown in Fig.8. For comparison, the QEPAS signals of the 100 ppm dry CH_4 are also plotted. The signal enhancement is not as high as in the case of using a nitrogen carrier [19]. At low pressures (< 300 Torr), the enhancement factor is only ~15%. With increasing pressure, the QEPAS signals from the dry and wet gases gradually overlap. However, the addition of water vapor strongly impacts the *Q* factor and *R* values of the QTF, as shown in Fig.5(dashed lines). The *Q* factor decreases from an initial range 30000-50000 to a final range of 27500-37500 and as a result, the *R* values increase from 53-86 kΩ to 70-95 kΩ, respectively.

Equation (1) was used to obtain the conversion efficiency $\varepsilon(p)$ as a function of pressure that is shown in Fig. 9. At pressures between 100 to 760 Torr, a higher total gas pressure does not help promote the V-T relaxation rate of CH_4. Instead, the conversion efficiency decreased towards higher pressures. The behavior of both $\varepsilon(p)$ values can be explained by the diffusion of the excited molecules to the QTF's prongs or the mR tube wall with subsequent V-T relaxation collisions. The mean diffusion path traveled by an excited CH_4 molecule was calculated in order to check if they are able to reach the tubes wall within a modulation period $t=1/f_0=30.5$ μs. The diffusion coefficient in the CH_4/H_2 mixture at $T=297$ K and atmospheric pressure (*P*atm) is $D_{12}=0.721$ cm^2/s [22]. Using the 2D diffusion formula ($\sqrt{<l^2>}=\sqrt{4D_{12}\frac{P\text{atm}}{P}t}$) [19], the diffusion path is 260 μm at 100 Torr, which is comparable with the mR radius of 290 μm. At 760 Torr, a diffusion path of ~100 μm is obtained. Taking into account the ~ 100 μm diameter of the laser beam and the 300 μm gap between two prongs of QTF, excited CH_4 molecules are still able to reach the QTF's prongs and release their vibrational energy. Hence, we can conclude that the observed higher conversion efficiency at low pressure CH_4/H_2 is most likely the result of diffusion. With increasing pressure, the diffusion effect decreases and the collision de-excitation process between CH_4 and H_2 molecules becomes gradually dominant. When considering H_2O

influence, it was determined that the conversion efficiency $\varepsilon(p)$ induced by H_2O vapor is not a constant for different pressures, but rather has a larger value at lower gas pressures. This can be explained by increased collisions between excited H_2O molecules and the mR tubes with the longer diffusion path, which further enhances the QEPAS signal.

The influence of the different H_2O vapor concentrations on the QEPAS signal was measured at the optimum pressure of 200 Torr as shown in Fig.10. A linear fit can be used for the experimental results in Fig.10, based on the model reported in Ref 19 as H_2O does not significantly promote vibrational deexcitation of CH_4 in H_2. Such a fit yields the relaxation time constant $\tau_0{}^{H}P_0$=23±1.7 μs Torr, which describes V-T relaxation rate due to CH_4/H_2O collisions. The obtained value is 2.5 times slower than in wet nitrogen. The linear fit can be used as the correction curve to derive the actual CH_4 concentration value when H_2O vapor is present in a gas mixture.

6. Optimization and sensitivity of the NH_3 detection channel

The NH_3 absorption line at 6528.76 cm^{-1} was selected as the target line for NH_3 detection based on data reported by Webber et al [23]. An example of the QEPAS spectra acquired with 50 ppm NH_3 at 50 Torr and 760 Torr H_2 is shown in Fig.3(b). The selected line merges with a weaker line at 6528.89 at pressures > 600 Torr. A similar optimization process of working gas pressure and wavelength modulation depth as was completed for CH_4 was carried out for the NH_3 channel. The results are shown in Fig.4(b). Unlike CH_4, which detected at an optimum pressure of ~200 Torr, the optimum pressure for NH_3 detection is 50 Torr. Subsequently, the NH_3 QEPAS signal decreased towards higher pressures until the two discrete absorption lines start to merge at 600 Torr. Similar plots of the *Q* factor and *R* values as observed for a dry CH_4/H_2 mixture were obtained. Based on the data in Fig.4(b) and *R* values calculated via Eq. (6), the SNR for the optimum laser current modulation amplitude was plotted in Fig. 6(b). The maximum SNR occurs at 50 Torr. However, the SNR has a second peak at pressures > 600 Torr regardless of the *Q* factor decrease. This enhancement results from an increase of the absorption coefficient due to the merging of two absorption lines, as shown in Fig. 3(b). Thus, we can operate the NH_3 channel at ambient atmospheric pressure with only a 1/4 loss of detection sensitivity.

The linearity and detection sensitivity of the NH_3 channel were evaluated by measuring its response to varying NH_3 concentrations in a 150 sccm H_2 flow. A gas standard generator (Kin-Tec) was employed to produce different NH_3 concentrations. The diode laser wavelength was locked to the center of the 6528.76 cm^{-1} NH_3 absorption line. The measurements were carried out at a pressure of 50 Torr. The results were recorded with a 1-s averaging time and are depicted in

Fig.11. At 50 Torr pressure, the measured R value is 47.6 Ω. With Δf=0.785 Hz, the calculated noise level for NH_3 detection is 5.2 μV. The scatter of consecutive measurements (noise level) is 5.1μV which is in good agreement with the predicted value. This noise level yields a noise-equivalent (1σ) concentration (NEC) of 1.27 ppm with a 1-s averaging time (0.785 Hz). The noise equivalent absorption coefficient is 9.1×10^{-9} $cm^{-1}W/\sqrt{Hz}$ normalized to a 50.2 mW optical power and a 0.785Hz detection bandwidth, which is comparable to a NEC value of 7.2×10^{-9} $cm^{-1}W/\sqrt{Hz}$ obtained in N_2.

The less distinct NH_3 linearity is due to the error introduced by the gas standard generator calibrated using N_2 and not H_2 as the carrier gas. Varying flow rates ranging from 20 sccm to 500 sccm were measured for the two sensing channels. No excessive flow noise was observed. Due to the fast V-T relaxation rate of NH_3 [20], the influence of water vapor as a V-T relaxer can be neglected.

In order to characterize long-term drifts and establish signal averaging limits, the results of the Allan deviation $\sqrt{\langle \sigma_A^2 \rangle}$, for the NH_3 channel are presented in Fig. 14. For this analysis, the laser frequency was locked to the NH_3 absorption line at 6528.76 cm^{-1}, and pure carrier gas H_2 was introduced into the ADM. The Allan deviation expressed in terms of ammonia concentration is depicted in Fig 12. The Allan deviation at the beginning closely follows a $1/\sqrt{t}$ dependence [24], which indicates that white Johnson noise of the QTF remains the dominant source of noise for time sequences of 1 to 200 s. However, the Allan deviation experiences a sensitivity drift when averaging exceed 600 s. Thus a stability period of 200-600 s and an optimum detection sensitivity of 100-150 ppb are determined. Since the same ADM and carrier gas are used for the CH_4 channel, the minimum Allan deviation of CH_4 is shifted only in the vertical direction. Hence, the CH_4 exhibits the same stability period as the NH_3 channel.

7. Conclusions

An outline for the detection of residuals CH_4 and NH_3 in impure hydrogen gas using QEPAS has been presented. Although a matched mR can improve the SNR for a QEPAS based sensor ~30 times, a non-matched mR is better suited for detection of impurities in hydrogen and enhances the SNR just ~10 times. However in hydrogen, the QTF has a relatively high Q factor. The reduction of the QEPAS signal associated with a non-matched mR is compensated by the high Q factor of the QTF when in a hydrogen carrier gas environment (ie with a Q factor ranging from a Q=55,000 at 50 Torr to a Q=30,000 at atmospheric pressure) compared to the Q in nitrogen (where the Q factor ranges from a 30,000 in 50 Torr to 2,000 at atmospheric pressure).

As a result, the sensitivity of the non-matched QEPAS configuration employed in H_2 can achieve comparable or increased detection sensitivity as an optimum QEPAS sensor configuration for N_2 with the additional benefit of a shorter mR length, which facilitates optical alignment of the optical coupling scheme from diode laser to ADM. The addition of H_2O does not significantly promote vibrational de-excitation of CH_4 in H_2, although it is efficient in the case of a CH_4/N_2 mixture. In the presence of high H_2O vapor concentrations (>2000 ppmv), a correction to the measured CH_4 concentration is necessary by monitoring the H_2O content. In addition, the optimal detection pressures for CH_4 and NH_3 do not coincide. When two gases are measured simultaneously in one sample gas, a pressure of 100 Torr was used. In this case each channel looses ~8% SNRs. The QEPAS response is directly proportional to the laser power. Therefore the NEC limits can be much lower if either a higher power diode laser source (or fiber amplified diode laser source) is used. In addition, the system allow useful data averaging for time periods long up to 200 s to obtain lower background noise level and improved detection sensitivity.

For a static gas measurement, it was found that the optical alignment of epoxied components in the QEPAS ADM is vulnerable to sudden large pressure changes. This issue can be solved by using solder processing, instead of epoxy processing, in mounting all ADM parts in the next generation of the ADM design. The CEU for the two target analytes can be preprogrammed to be capable of controlling the acquisition of up to 10 sets of QEPAS based sensor parameters. Each set includes the selection of the diode laser, reference cell, laser current and temperature settings, modulation depth and regulation parameters. Based on the function of CEU and a 4×4 MEM optical switch, the current two gas sensor design can be adapted to a multi-gas sensor by adding more commercially available CW TEC DFB diode lasers. The CEU can be programmed to loop through desired diode lasers in an autonomous mode, which leads a diode laser based sensor design that is compact, user friendly and cost effective.

ACKNOWLEDGEMENTS

The Rice University group acknowledges financial support from a National Science Foundation ERC MIRTHE award and a grant C-0586 from the Welch Foundation. Significant funding was also provided by the Department of Energy (DOE) National Nuclear Security Administration (NNSA) Readiness Campaign (NA-123).

REFERENCES

1 A.A. Kosterev, F.K. Tittel, D.V. Serebryakov, A.L. Malinovsky, I.V. Morozov, "Applications of quartz tuning forks in spectroscopic gas sensing", Rev. Sci. Instrum. **76**, 043105 (2005)

2 A.A. Kosterev, Y.A. Bakhirkin, R.F. Curl, F.K. Tittel, "Quartz-enhanced photoacoustic spectroscopy", Opt. Lett. **27**, 1902-1904 (2002)

3 L. Dong, A.A. Kosterev, D. Thomazy, F.K. Tittel, "QEPAS spectrophones: design, optimization, and performance", Appl. Phys. B **100**, 627-635 (2010)

4 A. Miklos, P. Hess, Z. Bozoki, "Application of acoustic resonators in photoacoustic trace gas analysis and metrology", Rev. Sci. Instrum. **72**, 1937-1955 (2001)

5 D.V. Serebryakov, I.V. Morozov, A.A. Kosterev, V.S. Letokhov, "Laser microphotoacoustic sensor of ammonia traces in the atmosphere", Quantum Electron. **40**, 167 (2010)

6 A. A. Kosterev, F. K. Tittel, "Ammonia detection by use of quartz-enhanced photoacoustic spectroscopy with a near-IR telecommunication diode laser", Appl. Opt. **43**, 6213-6217 (2004)

7 L. Dong, A. A. Kosterev, D. Thomazy, F. K. Tittel, "Compact Portable QEPAS Multi-gas Sensor", *Proc. of SPIE* **7945**: 50R-1 (2011)

8 D Weidmann, A. A Kosterev, F. K Tittel, N. Ryan, D. McDonald, "Application of a widely electrically tunable diode laser to chemical gas sensing with quartz-enhanced photoacoustic spectroscopy", Opt. Lett. **29**, 1837-1839 (2004)

9 A.A. Kosterev, L. Dong, D. Thomazy, F.K. Tittel, S. Overby, "QEPAS for chemical analysis of multi-component gas mixtures", App. Phys. B **101**, 649-659 (2010)

10 S Schilt, Anatoliy A Kosterev, Frank K Tittel, "Performance evaluation of a near infrared QEPAS based ethylene sensor", Appl. Phys. B **95,** 813-824 (2009)

11 L. Dong, V. Spagnolo, R. Lewicki, F. K. Tittel, "Ppb-level detection of nitric oxide using an external cavity quantum cascade laser based QEPAS sensor", Opt. Express, submitted

12 V. Spagnolo, A. A. Kosterev, L. Dong, R. Lewicki, F. K. Tittel, "NO trace gas sensor based on quartz enhanced photoacoustic spectroscopy and external cavity quantum cascade laser", App. Phys. B **100,** 125-130 (2010)

13 A. A Kosterev, Y. A. Bakhirkin, F. K. Tittel, "Ultrasensitive gas detection by quartz-enhanced photoacoustic spectroscopy in the fundamental molecular absorption bands region", Appl. Phys. B **80,** 133-138 (2005)

14 R. Lewicki, A. A. Kosterev, D. M. Thomazy, T. H. Risby, S. Solga, T. B. Schwartz, F. K. Tittel, "Real time ammonia detection in exhaled human breath using a distributed feedback quantum cascade laser based sensor", *Proc. of SPIE* **7945**: 50K-2 (2011)

15 A K Ngai, S T Persijni, D Lindsay, Anatoliy A Kosterev, P Gross, C J Lee, C M Cristescu, Frank K Tittel, K J Boller, F J Harren, "Continuous Wave Optical Parametric Oscillator for Quartz-Enhanced Photoacoustic Trace Gas Sensing", Appl. Phys. B **89,** 123-128 (2007)

16 M. Horstjann, Y. A Bakhirkin, A. A. Kosterev, R. F. Curl, F. K. Tittel, C. M. Wong, C. J. Hill, R. Q. Yang, "Formaldehyde sensor using interband cascade laser based quartz-enhanced photoacoustic spectroscopy", Appl. Phys. B **79,** 799-803 (2004)

17 A. A. Kosterev, P. R. Buerki, L. Dong, M. Reed, T. Day, F. K. Tittel, "QEPAS detector for rapid spectral measurements." App. Phys. B **100,** 173-180 (2010)

18 R. C. Weast, M. J. Astle, *CRC Handbook of Chemistry and Physics* (61st Edition 1980-1981, Boca Raton, Florida)

19 A. A. Kosterev, Y.A. Bakhirkin, F.K. Tittel, S. Mcwhorter, B. Ashcraft, "QEPAS methane sensor performance for humidified gases", Appl. Phy. B **92**, 103-109 (2008)

20 T. L. Cottrell, J. C. McCoubrey, *Molecular energy transfer in gases* (London Butterworths, 1961)

21 A.A. Kosterev, T.S. Mosely, F.K. Tittel, "Impact of humidity on quartz-enhanced photoacoustic spectroscopy based detection of HCN", Appl. Phy. B 85, 295-300 (2006)

22 C. R. Wilke, C. Y. Lee, "Estimation of diffusion coefficients for gases and vapors", Ind. Eng. Chem **47**, 1253-1257 (1955)

23 M. E. Webber, M. Pushkarsky, C. K. N. Patel, “Fiber-amplifier-enhanced photoacoustic spectroscopy with near-infrared tunable diode lasers”, Appl. Opt. **42**, 2119-2126 (2003)
24 P. Werle, “Accuracy and precision of laser spectrometers for trace gas sensing in the presence of optical fringes and atmospheric turbulence”, Appl. Phys. B 102, 313-329 (2011)

Figure Captions

Fig. 1 Fiber-coupled QEPAS acoustic detection module (ADM).

Fig. 2 Schematic of a compact two-gas QEPAS sensor. TS, PS, HS—temperature, pressure, and humidity sensors, ADM — acoustic detection module, TA — transimpedance amplifier, DL1, DL2—diode lasers, CEU—control electronics unit

Fig. 3 (a) QEPAS spectra of the CH_4 lines acquired at a 100 ppmv CH_4 concentration and 200 Torr H_2. (A=5 mA, Δf=0.785 Hz). (b) QEPAS spectra of the NH_3 lines for a 50 ppmv NH_3 concentration acquired at 50 Torr and 760 Torr, respectively. (A=7 mA for 50 Torr, A=33 mA for 760 Torr, Δf=0.785 Hz)

Fig. 4 (a) QEPAS signal corresponding to the peak CH_4 absorption near 6057.1 cm^{-1} as functions of WM depth and current modulation amplitude acquired at different pressures. (b) QEPAS signal corresponding to the peak NH_3 absorption near 6528.76 cm^{-1} as functions of WM depth and current modulation amplitude acquired at different pressures.

Fig. 5 Solid lines: measured Q factor and R values in dry H_2 as a function of pressures. Dashed lines: measured Q factor and R values in H_2 with 2.29% H_2O vapor at different gas pressures.

Fig. 6 (a) Plot of the QEPAS maximum signal amplitude and signal-to-noise ratio of CH_4 as a function of pressures. Each curve is normalized to its maximum value. (b) SNR with optimum laser current modulation amplitude for a 50 ppmv NH_3 in H_2 mixture and a 1-s averaging time.

Fig. 7 (a) QEPAS signal repetitively recorded while the CH_4 concentration was varied by changing gas cylinders with different calibrated CH_4 concentrations. (b) Same data averaged and plotted as a function of certified concentration of CH_4 gas cylinders.

Fig. 8 Measured QEPAS signals for 100 ppm CH_4 in dry H_2 and H_2 with 2.29% H_2O vapor as a function of total gas pressure.

Fig. 9 Efficiency of the optical radiation-to-sound conversion $\varepsilon(p)$ as a function of total pressures for CH_4 in dry H_2 and H_2 with 2.29% H_2O vapor.

Fig. 10 QEPAS signal as a function of H_2O concentration in a CH_4/H_2 mixture with a linear fit.

Fig. 11 (a) QEPAS signal acquired repetitively while the CH_4 concentration was varied by changing of the carrier gas flow using a standard gas generator. (b) same data averaged and plotted as a function of the calibration of the standard gas generator.

Fig. 12 Alan deviation as a function of the data averaging period. Solid circles trace: laser is locked to the NH_3 absorption line, data acquisition time 1 s. Dashed line: $1/\sqrt{t}$ slope. Dotted line: $\sqrt{t}$ slope

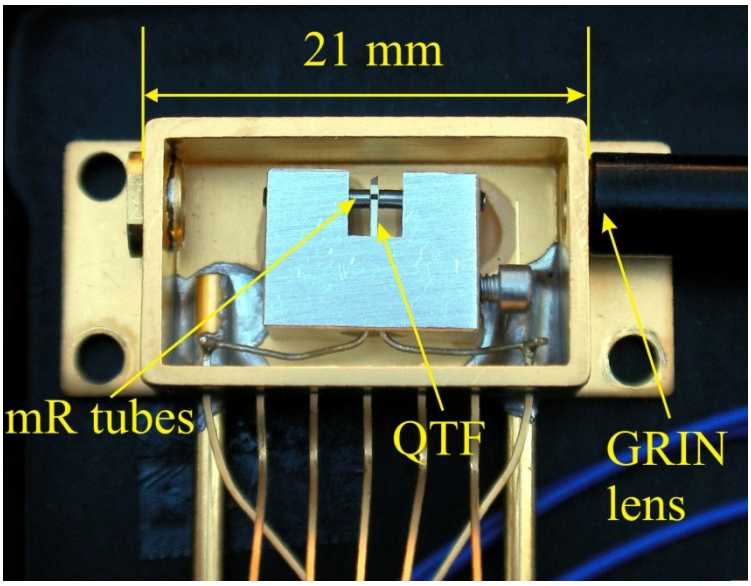
21 mm
mR tubes
QTF
GRIN
lens

Fig.1

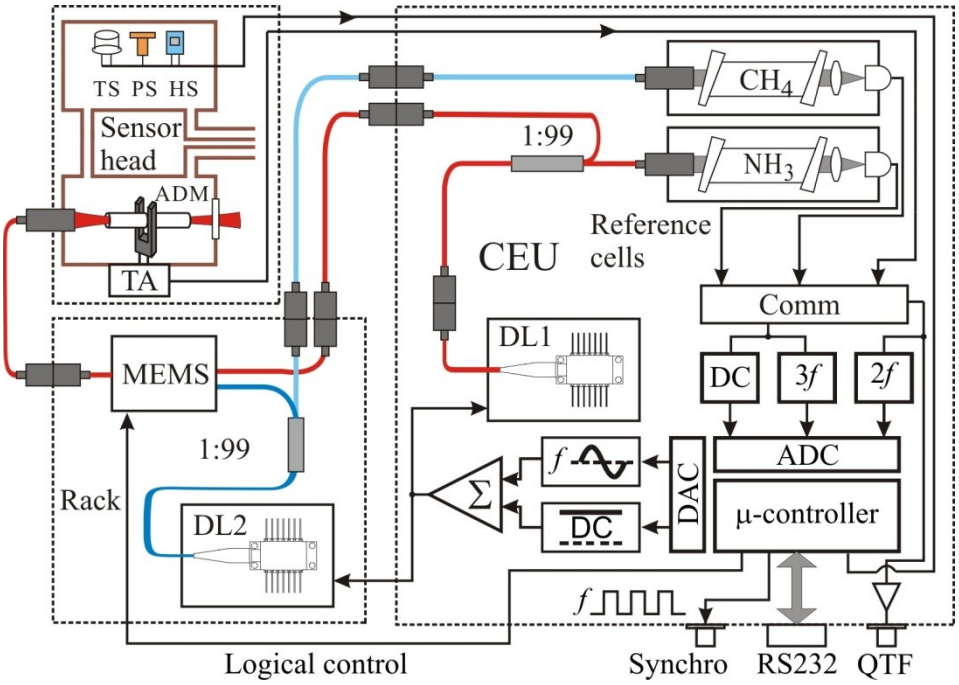
TS PS HS
Sensor
head
ADM
TA
MEMS
1:99
Rack
DL2
CEU
1:99
DL1
Reference
cells
CH4
NH3
Comm
DC
3f
2f
ADC
μ-controller
DAC
f
DC
Σ
f
Logical control
Synchro
RS232
QTF

Fig.2

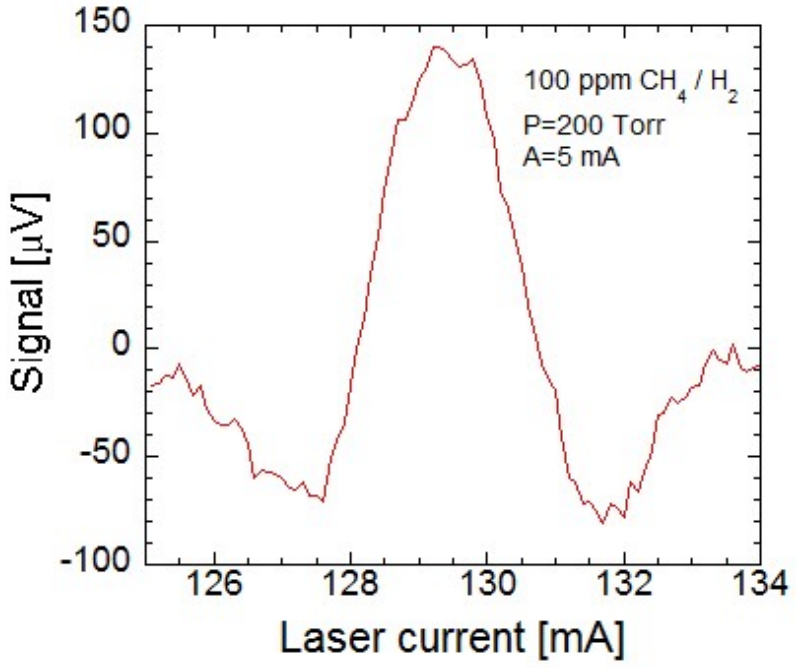
100 ppm CH4 / H2
P=200 Torr
A=5 mA
Signal [μV]
Laser current [mA]
150
100
50
0
-50
-100
126
128
130
132
134

Fig. 3 (a)

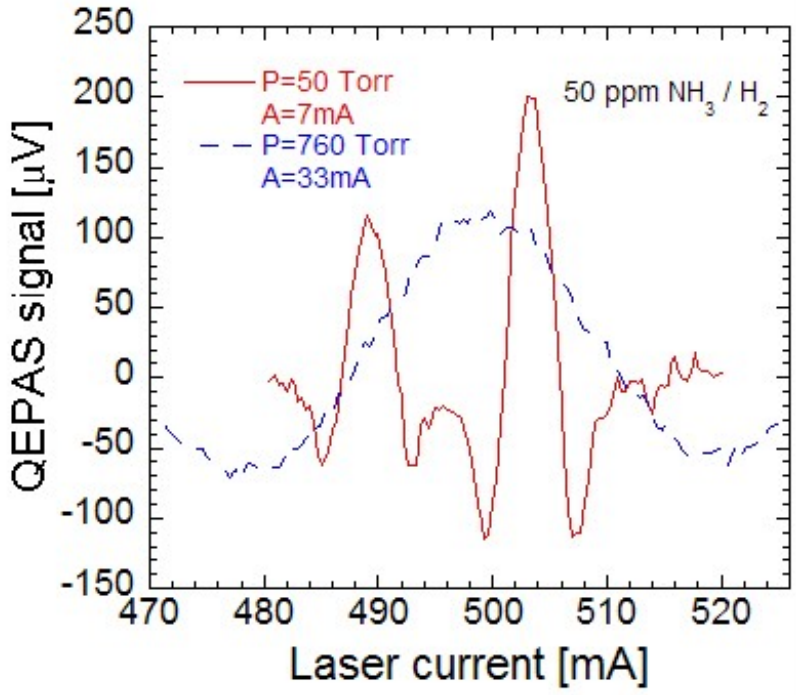
P=50 Torr
A=7mA
P=760 Torr
A=33mA
50 ppm NH3 / H2
QEPAS signal [μV]
Laser current [mA]
250
200
150
100
50
0
-50
-100
-150
470
480
490
500
510
520

Fig. 3 (b)

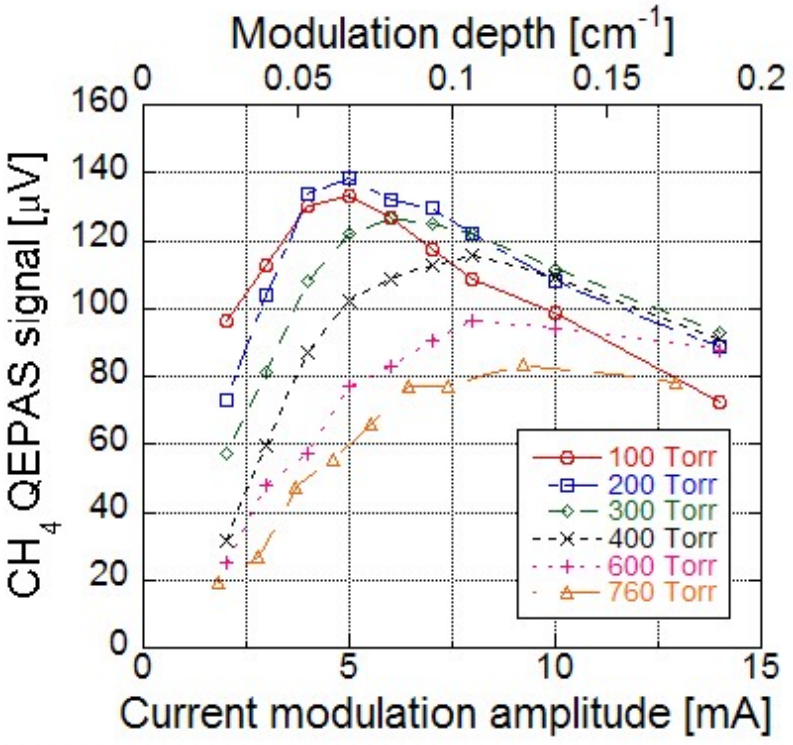
Modulation depth [cm^{-1}]
0
0.05
0.1
0.15
0.2
160
140
120
100
80
60
40
20
0
CH$_4$ QEPAS signal [μV]
0
5
10
15
Current modulation amplitude [mA]
100 Torr
200 Torr
300 Torr
400 Torr
600 Torr
760 Torr

Fig. 4 (a)

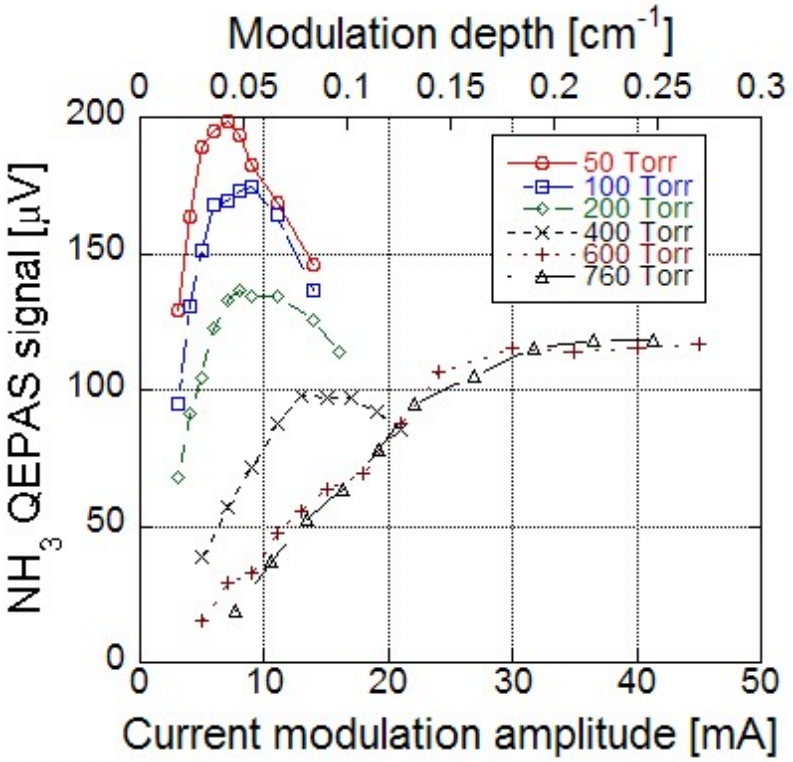
Modulation depth [cm^{-1}]
0
0.05
0.1
0.15
0.2
0.25
0.3
200
150
100
50
0
NH$_3$ QEPAS signal [μV]
0
10
20
30
40
50
Current modulation amplitude [mA]
50 Torr
100 Torr
200 Torr
400 Torr
600 Torr
760 Torr

Fig. 4 (b)

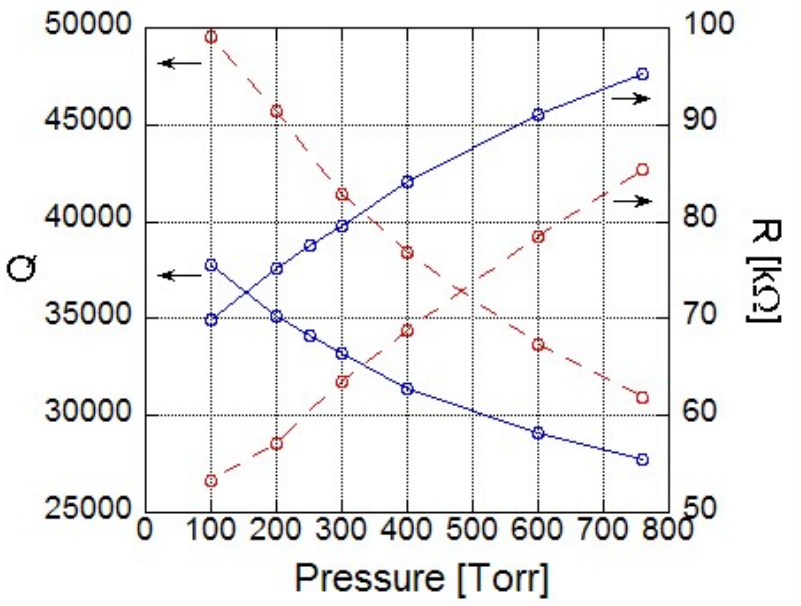
50000
45000
40000
35000
30000
25000
Q
100
90
80
70
60
50
R [kΩ]
0
100
200
300
400
500
600
700
800
Pressure [Torr]

Fig. 5

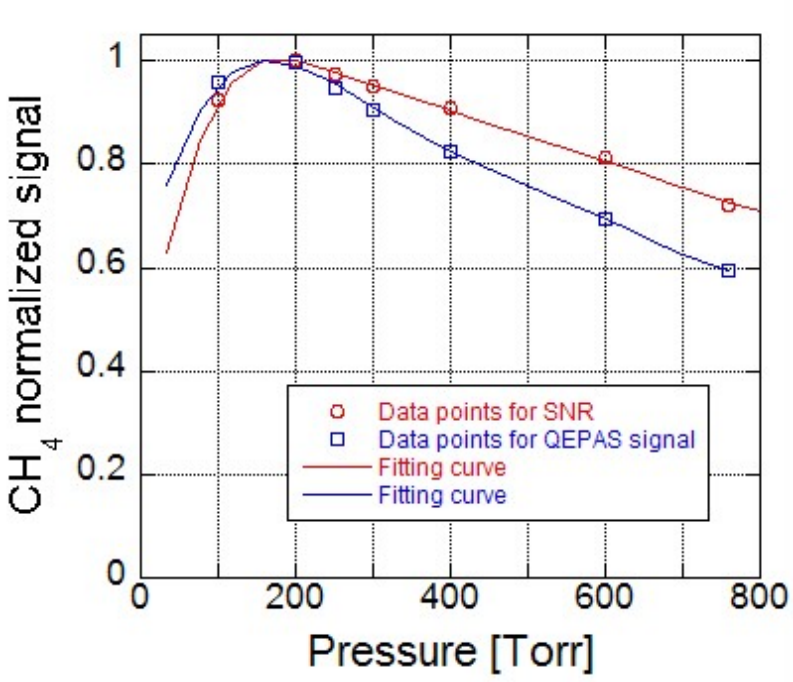
1
0.8
0.6
0.4
0.2
0
CH4 normalized signal
Data points for SNR
Data points for QEPAS signal
Fitting curve
Fitting curve
0
200
400
600
800
Pressure [Torr]

Fig. 6 (a)

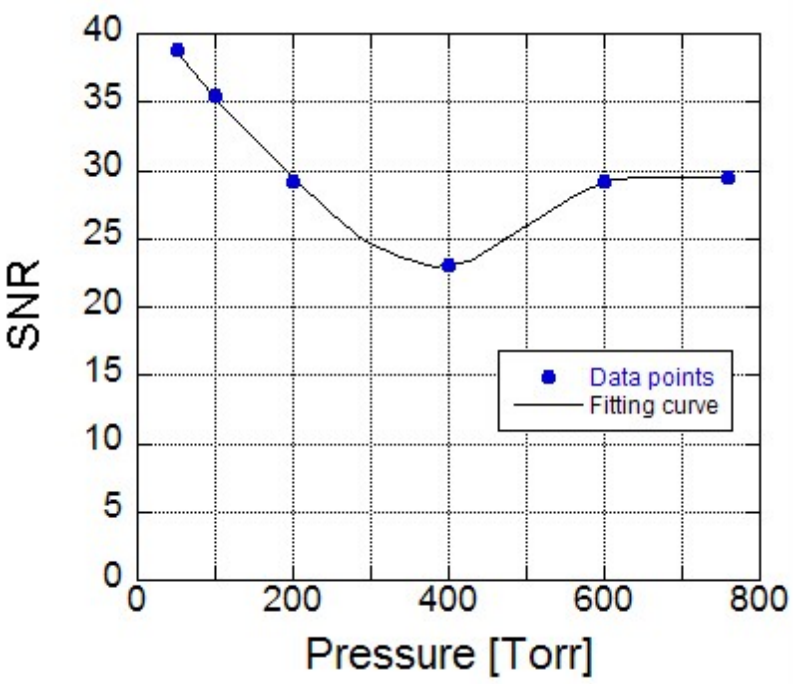
SNR
Pressure [Torr]
Data points
Fitting curve
0
5
10
15
20
25
30
35
40
0
200
400
600
800

Fig. 6 (b)

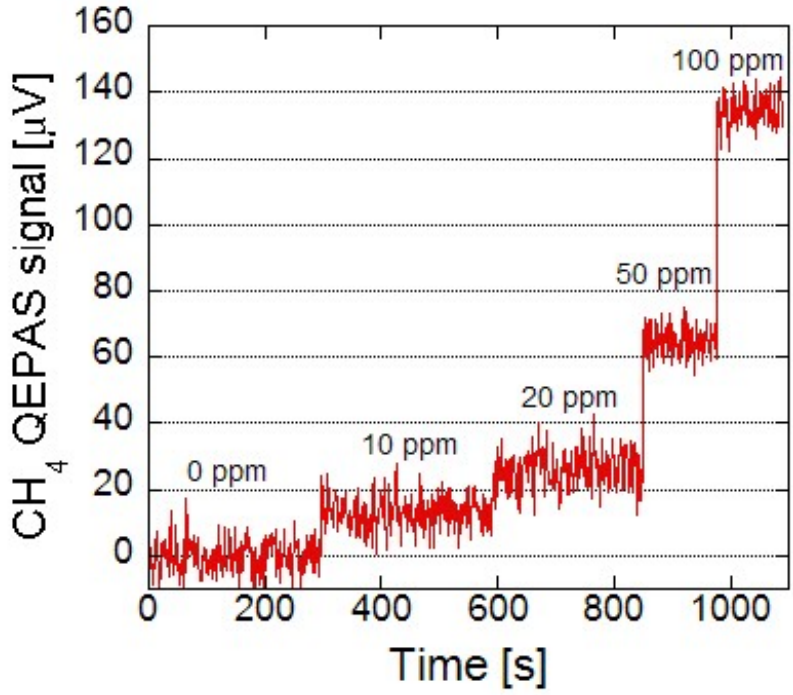
CH4 QEPAS signal [μV]
Time [s]
0 ppm
10 ppm
20 ppm
50 ppm
100 ppm
0
20
40
60
80
100
120
140
160
0
200
400
600
800
1000

Fig. 7 (a)

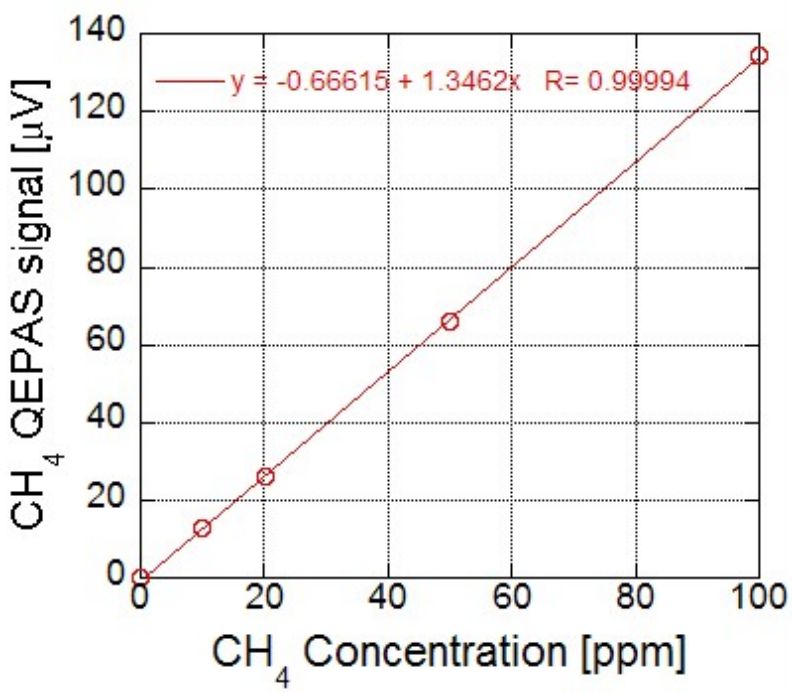
y = -0.66615 + 1.3462x R= 0.99994
CH4 QEPAS signal [μV]
CH4 Concentration [ppm]
0
20
40
60
80
100
120
140

Fig. 7 (b)

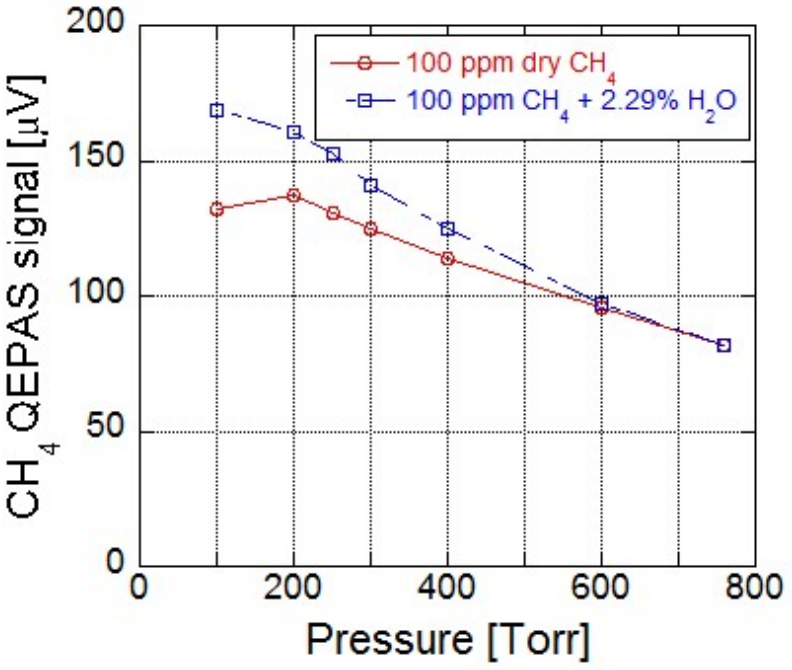
100 ppm dry CH4
100 ppm CH4 + 2.29% H2O
CH4 QEPAS signal [μV]
Pressure [Torr]
0
50
100
150
200
0
200
400
600
800

Fig. 8

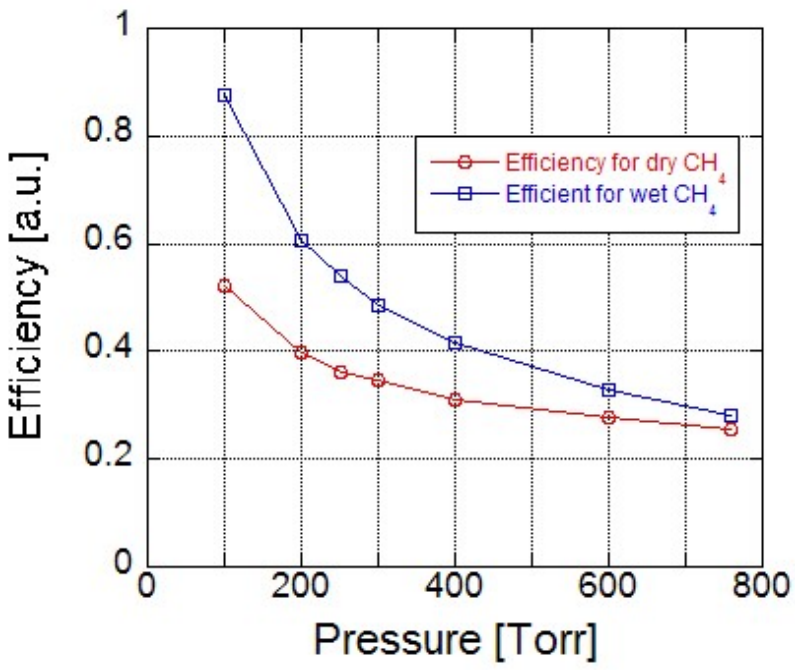
Efficiency [a.u.]
Pressure [Torr]
Efficiency for dry CH4
Efficient for wet CH4
0
0.2
0.4
0.6
0.8
1
0
200
400
600
800

Fig. 9

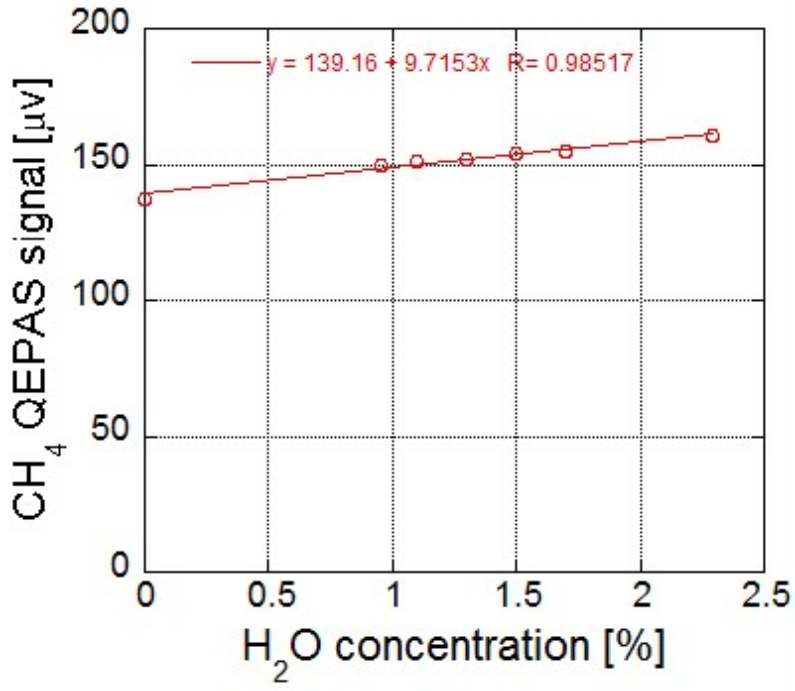
CH4 QEPAS signal [μV]
H2O concentration [%]
y = 139.16 + 9.7153x R= 0.98517
0
50
100
150
200
0
0.5
1
1.5
2
2.5

Fig. 10

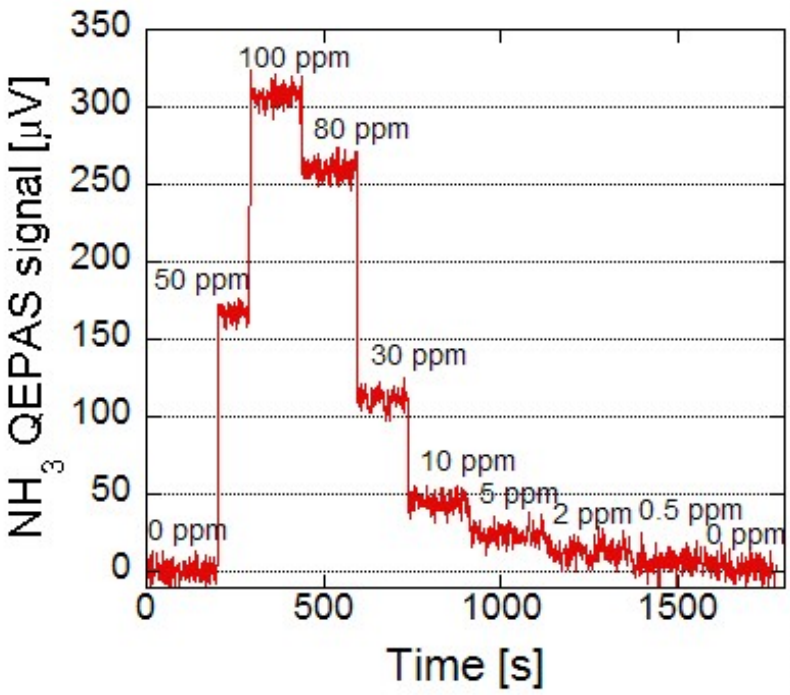

Fig. 11 (a)

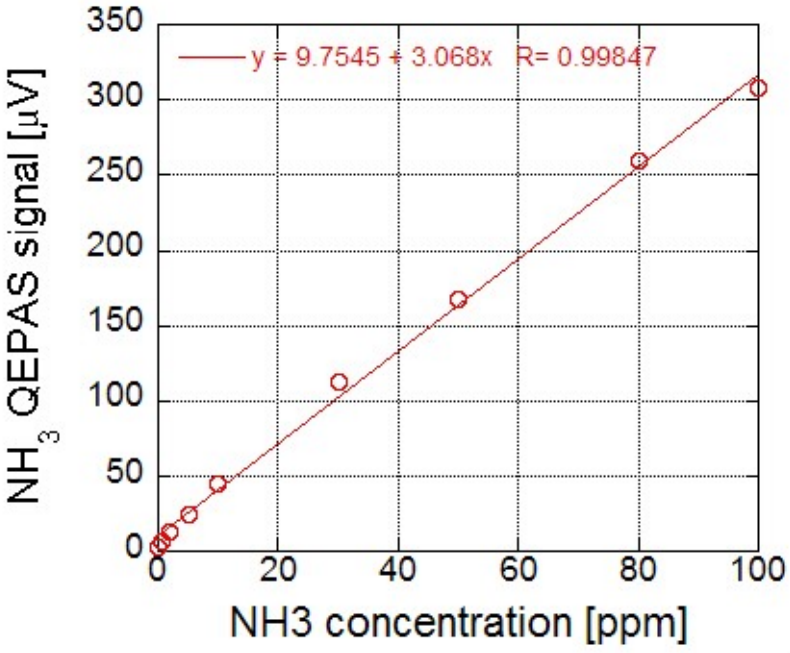

Fig. 11 (b)

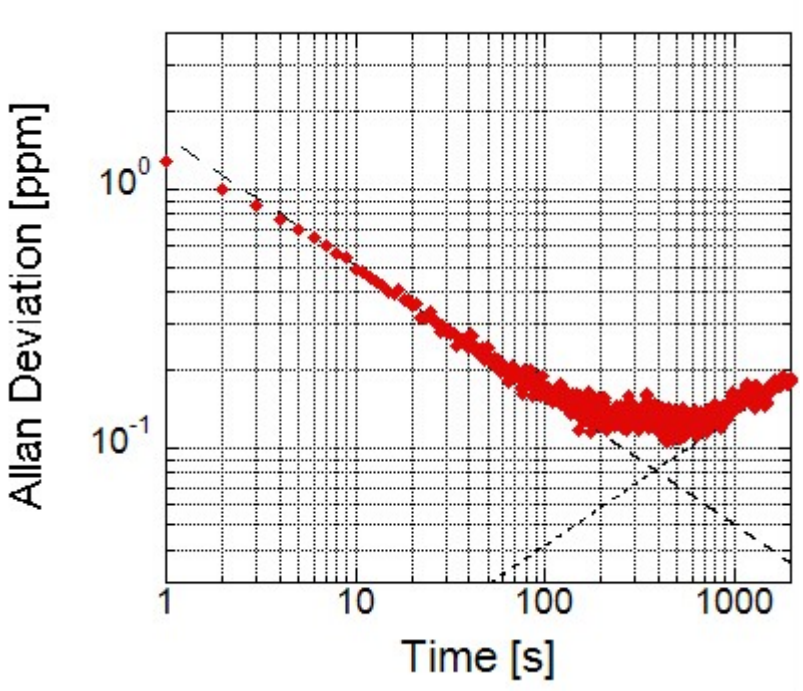

Fig. 12